Adaptive Finite Elements for Monolithic Fluid-Structure Interaction on a Prolongated Domain: Applied to an Heart Valve Simulation

Thomas Wick[1]*

[1] *Institute of Applied Mathematics, University of Heidelberg*
INF 293/294, 69120 Heidelberg, Germany
e-mail: thomas.wick@iwr.uni-heidelberg.de

Abstract

In this work, we apply a fluid-structure interaction method to a long axis heart valve simulation. Our method of choice is based on a monolithic coupling scheme for fluid-structure interaction, where the fluid equations are rewritten in the 'arbitrary Lagrangian Eulerian' framework. To prevent back-flow of waves in the structure due to its hyperbolic nature, a damped structure equation is solved on an artificial layer that prolongates the computational domain. This coupling is stable on the continuous level. To reduce the increased computational cost in presence of the artificial layer, we refine the mesh only regions of interest. To this end, a stationary version of goal-oriented mesh refinement is part of our numerical tests. The results show that heart valve dynamics can be simulated with our proposed model.

Keywords: bio-mechanics, blood flow, finite element method, fluid-structure interaction, goal-oriented mesh adaption

1. Introduction

Cardiovascular diseases represent a major part on the mortality in industrialized countries. For this reason, there is an increasing demand from the medical community for rigorous and quantitative investigations of the human cardiovascular system [21, 18]. However, the complexity of the circulatory system makes modeling and simulation challenging because there are many fundamental ingredients taking into account.

In this work, we focus on a main component of the circulatory system: the heart. More specifically, we are interested in modeling and simulation of the aortic heart valve, which pumps oxygenated blood from the left ventricle in the aorta. Such processes imply the interaction of blood with the heart walls and the vessel walls. The mathematical method of choice to construct appropriate models and simulations is the fluid-structure interaction approach. Beyond that, fluid-structure interaction have significant influence in bio-mechanics [10, 19, 21, 16].

There exist various approaches to model heart valve dynamics. Usually, they are considered as fluid-structure interaction problems that can be solved by different solution approaches [17, 24, 20, 23, 25]. Here, we use the 'arbitrary Lagrangian-Eulerian' framework (ALE) that is frequently used in the literature to model fluid-structure interaction problems.

The problem is solved by a monolithic solution algorithm because one has to overcome the well-known added-mass effect that occurs when the density of fluid and structure are of same order like in hemodynamics [7]. In addition, a closed setting for the equations is necessary for rigorous goal-oriented error estimation [4]; that is explained below for a stationary case.

By construction, the ALE approach is not capable to model topological changes, which occur when two valves touch each other. However, this point is of less importance in our studies, because we focus on boundary conditions for the structure on the outflow section. This subject should not be neglected because the radius of the aorta may vary in a range of $5-10$ per cent between diastole and systole (the two phases in a cardiac cycle) [21]. This is a large displacement of the blood vessel wall that effects both the flow field and the blood vessel dynamics itself.

In the last years, a lot of effort has been spent to model appropriate descriptions for fluid and pressure conditions on the artificial outflow boundary [13, 12, 16, 11], which are related to the flow field. Consideration of appropriate structure conditions becomes important when dealing with large deflections of the blood vessel walls. In particular, we are interested in the capability to absorb outgoing waves (i.e. energy) to prevent back flow of waves.

To the best of our knowledge, this topic is novel and others have just begun with investigations [14]. Here, the authors consider flow rate conditions of the fluid problem and a complete set of (non-defective) boundary conditions for the structure problem on the artificial outflow section.

Originally, energy absorption problems arise in acoustic and electromagnetic wave propagation [2, 9]. Various approximate boundary conditions have been used to absorb incoming waves. For complex situations they have some major disadvantages, for instance, accumulation of error contributions over the whole time interval. To avoid these problems, higher order derivatives of the problem at hand can be used, which makes implementation difficult. Another approach to eliminate reflections was suggested by appending an artificial layer to the computational domain. This layer is supposed to absorb the waves. Especially, one can use a perfectly matched layer (PML) [3]. We employ this idea to extend the computational domain that is used to absorb the outgoing waves for our fluid-structure interaction problem.

The major disadvantage of this approach is higher computational cost due to solving both the complete fluid equations and structure equations on an artificial domain. To overcome this drawback, we could solve reduced equations in the artificial layer; or using an initial coarser mesh in the artificial part; or refining the mesh automatically during the solution process, but only in regions of interest . We present a combination of the two latter issues. For unsteady test cases, we coarsen the initial mesh by hand in the artificial domain. Moreover, we apply the

* The financial support by the DFG (Deutsche Forschungsgemeinschaft) and the Heidelberg Graduate School HGS MathComp is gratefully acknowledged. Further, the author thanks Jeremi Mizerski for fruitful discussions.

Dual Weighted Residual (DWR) method to drive an automatic mesh adaption during the solution process [4]. This approach is challenging for time-dependent coupled problems and still under investigation [8, 22, 29]. For this reason, we only test a simplified version, to verify if the method is capable to deal with heart valve configurations.

The paper is organized as follows: In Section 2, we describe the equations for both the fluid and structure, including a damped hyperbolic equation. After, we formulate the problem in a monolithic setting. Section 3 is devoted to a brief description of the discretization process. In addition, we state a stabilization technique for the convective term that is based on streamline diffusion. Temporal discretization is based on the shifted Crank-Nicolson scheme, for spatial discretization a Galerkin finite element approach is used. A Newton method is applied to solve the non-linear system. In Section 4, we introduce the DWR method that is used as an indicator for goal-oriented mesh adaption. In the last section, numerical tests will be presented to exemplify our proposed methods. The parameters for both the material and geometry are taken from literature and were discussed with a medical doctor.

2. Fluid-structure problem

We introduce some notation and study the interaction of an incompressible Newtonian fluid and a structure of hyperbolic type [13].

2.1. Notation

We denote by $\Omega \subset R^d$, $d = 2, 3$, the domain of the fluid-structure interaction problem. This domain is supposed to be time independent but consists of two time dependent subdomains $\Omega_f(t)$ and $\Omega_s(t)$. The interface between both domain is denoted by $\Gamma_i(t) = \partial\Omega_f(t) \cap \partial\Omega_s(t)$. The initial (or later reference) domains are denoted by $\widehat{\Omega}_f$ and $\widehat{\Omega}_s$, respectively, with the interface $\widehat{\Gamma}_i$. Further, we denote the outer boundary with $\partial\widehat{\Omega} = \widehat{\Gamma} = \widehat{\Gamma}_D \cup \widehat{\Gamma}_N$ where $\widehat{\Gamma}_D$ and $\widehat{\Gamma}_N$ denote Dirichlet and Neumann boundaries, respectively.

We adopt standard notation for the usual Lebesgue and Sobolev spaces and their extensions by means of the Bochner integral for time dependent problems [28]. We use the notation $(\cdot,\cdot)_X$ for a scalar product on a Hilbert space X and $\langle\cdot,\cdot\rangle_{\partial X}$ for the scalar product on the boundary ∂X. For the time dependent functions on a time interval I, the Sobolev spaces are defined by $\mathcal{X} := L^2(I; X)$. Concretely, we use $\mathcal{L} := L^2(I; L^2(\Omega))$ and $\mathcal{V} := H^1(I; H^1(\Omega)) = \{v \in L^2(I; H^1(\Omega)) : \partial_t v \in L^2(I; H^1(\Omega))\}$.

2.2. The coupled problem

The equations for fluid and structure are defined in their natural frameworks. The fluid problem reads:

$$\begin{aligned} \rho_f\, \partial_t \boldsymbol{v}_f|_{\hat{\mathcal{A}}} + \rho_f(\boldsymbol{v}_f - \boldsymbol{w})\cdot\boldsymbol{\nabla}\boldsymbol{v}_f - \mathbf{div}\boldsymbol{\sigma_f} = \mathbf{0} \quad &\text{in } \Omega_f(t),\\ \mathrm{div}\boldsymbol{v}_f = 0 \quad &\text{in } \Omega_f(t),\\ \boldsymbol{v}_f = \boldsymbol{v}^D \quad \text{on } \Gamma_{f,\text{in}}(t), \quad \boldsymbol{\sigma}\boldsymbol{n}_f = \boldsymbol{g}_{f,N} \quad &\text{on } \Gamma_{f,\text{out}}(t). \end{aligned} \tag{1}$$

with the Cauchy stress tensor $\boldsymbol{\sigma_f}$. The (undamped) structure problem is defined by:

$$\begin{aligned} \hat{\rho}_s\partial_t^2\hat{\boldsymbol{u}}_s - \widehat{\mathbf{div}}(\widehat{\boldsymbol{F}}\widehat{\boldsymbol{\Sigma}}_s) = \mathbf{0} \quad &\text{in } \widehat{\Omega}_s,\\ \hat{\boldsymbol{u}}_f = \mathbf{0} \quad \text{on } \widehat{\Gamma}_{s,D}, \quad \widehat{\boldsymbol{F}}\widehat{\boldsymbol{\Sigma}}_s\boldsymbol{n}_s = \mathbf{0} \quad &\text{on } \widehat{\Gamma}_i. \end{aligned} \tag{2}$$

with the second Piola-Kirchhoff tensor $\widehat{\boldsymbol{\Sigma}}_s$ and the deformation gradient $\widehat{\boldsymbol{F}}$. The coupling conditions are given by (with $\det(\widehat{\boldsymbol{F}}) = J$):

$$\begin{aligned} &\hat{\boldsymbol{u}}_f = \mathrm{Ext}(\hat{\boldsymbol{u}}_{\boldsymbol{s}}|_{\widehat{\boldsymbol{\Gamma}}_{\boldsymbol{i}}}), \quad \Omega_f(t) = \hat{\mathcal{A}}(\widehat{\Omega}_f, t), \quad \hat{\boldsymbol{w}} = \partial_t\hat{\boldsymbol{u}}_f \text{ in } \widehat{\Omega}_f,\\ &\hat{\boldsymbol{v}}_{\boldsymbol{f}} = \hat{\boldsymbol{w}} \text{ on } \Gamma_i(t), \quad \widehat{\boldsymbol{F}}\widehat{\boldsymbol{\Sigma}}_s\boldsymbol{n}_s + \hat{J}_f\hat{\boldsymbol{\sigma}}\hat{\boldsymbol{F}}_{\boldsymbol{f}}^{-\boldsymbol{T}}\hat{\boldsymbol{n}}_f = 0 \text{ on } \widehat{\Gamma}_i. \end{aligned} \tag{3}$$

The stress tensors, $\boldsymbol{\sigma}_f$ and $\widehat{\boldsymbol{\Sigma}}_s$, are defined as

$$\begin{aligned} &\boldsymbol{\sigma}_f := -p_f\boldsymbol{I} + \rho_f\nu_f(\boldsymbol{\nabla}\boldsymbol{v}_f + \boldsymbol{\nabla}\boldsymbol{v}_f^T),\\ &\widehat{\boldsymbol{\Sigma}}_s := (\lambda_s(\mathrm{tr}\widehat{\boldsymbol{E}})\boldsymbol{I} + 2\mu_s\widehat{\boldsymbol{E}}),\ \widehat{\boldsymbol{E}} = \frac{1}{2}(\widehat{\boldsymbol{F}}^T\widehat{\boldsymbol{F}} - I). \end{aligned}$$

The viscosity and the density of the fluid are denoted by ν_f and ρ_f, respectively. The elastic structure is characterized by the Lamé coefficients μ_s, λ_s.

The principal unknowns are the fluid velocity $\hat{\boldsymbol{v}}_f : \widehat{\Omega}_f \times R^+ \to R^3$, the fluid pressure $\hat{p} : \widehat{\Omega}_f \times R^+ \to R$, the structure displacement $\hat{\boldsymbol{u}}_s : \widehat{\Omega}_s \times R^+ \to R^3$, and the fluid domain displacement (mesh motion) $\hat{\boldsymbol{u}}_f : \widehat{\Omega}_f \times R^+ \to R^3$. The ALE mapping is denoted by $\hat{\mathcal{A}}$ and transforms the reference configuration $\widehat{\Omega}_f$ of the fluid to the physical domain $\Omega_f(t)$. The variable $\hat{\boldsymbol{w}}$ defines the fluid domain velocity. Furthermore, any function $\hat{q} \in \hat{\Omega}$ is defined on Ω by $q(x) = \hat{q}(\hat{x})$ for $x = \hat{\mathcal{A}}(\hat{x}, t)$.

2.3. Construction of the ALE mapping

The fluid mesh motion is reconstructed by posing an additional equation that is driven by the motion of the interface $\Gamma_i(t)$, i.e., $\hat{\mathcal{A}} = \hat{\boldsymbol{u}}_s$ on $\widehat{\Gamma}_i$, leading to $\hat{\boldsymbol{w}} = \hat{\boldsymbol{v}}_s$ on $\widehat{\Gamma}_i$. Further, we fix the inlet and outlet boundary parts by $\hat{\boldsymbol{u}}_f = 0$ on $\widehat{\Gamma}_{f,\text{inlet}} \cup \widehat{\Gamma}_{f,\text{outlet}}$. In the fluid domain $\widehat{\Omega}_f$ the transformation $\hat{\mathcal{A}}$ is arbitrary but should satisfy certain regularity conditions (C^1-diffeomorphism) [13]. In particular, the fluid mesh is constructed by solving an harmonic problem (for stationary configurations) or a biharmonic equation (for large mesh deformations without re-meshing). We solve:

$$\begin{cases} \Delta\hat{\boldsymbol{u}}_f = 0 \quad \text{in } \widehat{\Omega}_f & \text{(harmonic)},\\ \Delta^2\hat{\boldsymbol{u}}_f = 0 \quad \text{in } \widehat{\Omega}_f & \text{(biharmonic)}, \end{cases}$$

$$\begin{cases} \hat{\boldsymbol{u}}_f = 0 \quad \text{on } \widehat{\Gamma}_{f,\text{inlet}} \cup \widehat{\Gamma}_{f,\text{outlet}} & \text{(harmonic)},\\ \hat{\boldsymbol{u}}_f = \partial_n\hat{\boldsymbol{u}} = 0 \quad \text{on } \widehat{\Gamma}_{f,\text{inlet}} \cup \widehat{\Gamma}_{f,\text{outlet}} & \text{(biharmonic)} \end{cases}$$

$$\left\{\hat{\boldsymbol{u}}_f = \hat{\boldsymbol{u}}_s \quad \text{on } \widehat{\Gamma}_i.\right.$$

2.4. Considerations on the damped wave equation

In the last years, a lot of effort has been spent in modeling appropriate boundary conditions for the fluid and pressure for the inlet and outlet boundaries [21, 11, 13, 14]; and many references cited therein. To overcome this deficiency, we prolongate the computational domain. Second, it is not clear which boundary conditions should be imposed for the structure on the outlet part. In the artificial extension of the computational domain, therefore, we use a damped version of the structure equations, to absorb incoming waves preventing structure reflections.

The modified structure problem in the extended domain $\widehat{\Omega}_s^{\text{ext}}$ is defined by:

$$\hat{\rho}_s\partial_t^2\hat{\boldsymbol{u}}_s - \widehat{\mathbf{div}}(\hat{\boldsymbol{F}}_s\widehat{\boldsymbol{\Sigma}}) + \gamma_w\partial_t\hat{\boldsymbol{u}}_s - \gamma_s\partial_t\widehat{\mathbf{div}}(\hat{\boldsymbol{F}}_s\widehat{\boldsymbol{\Sigma}}) = \mathbf{0},$$

with $\gamma_s, \gamma_w \geq 0$. Here, the first damping terms is referred to 'weak damping' whereas the second one is called by 'strong damping' because the full operator is used for damping.

In the following, we pose a standard mixed formulation of the structure equations in $\widehat{\Omega}_s^{\text{ext}}$:

$$\begin{aligned} \hat{\rho}_s\partial_t\hat{\boldsymbol{v}}_s - \widehat{\mathbf{div}}(\hat{\boldsymbol{F}}_s\widehat{\boldsymbol{\Sigma}}) + \gamma_w\hat{\boldsymbol{v}}_s - \gamma_s\partial_t\widehat{\mathbf{div}}(\hat{\boldsymbol{F}}_s\widehat{\boldsymbol{\Sigma}}) = \mathbf{0},\\ \hat{\rho}_s\partial_t\hat{\boldsymbol{u}}_s - \hat{\boldsymbol{v}}_s = \mathbf{0}, \end{aligned} \tag{4}$$

Remark 2.1. The modified structure Problem 4 reduces to the original Problem 2 by setting the damping parameters to $\gamma_w = \gamma_s = 0$. Therefore, we are dealing in the following only with Problem 4 in $\widehat{\Omega}_s$.

2.5. Stability of the coupled problem

In this section, we discuss the stability and give an extension of the a priori energy balance result for the coupled problem [13], chapter 9. We work in a monolithic framework where the interface conditions are exactly balanced. The energy loss in time is due to the fluid viscosity and the damping terms in the wave equation.

Proposition 2.1. *We assume that the conditions* $\boldsymbol{v_f} = \mathbf{0}$ *on* $\partial\Omega_f(t)\backslash\Gamma_i(t)$*, and* $\hat{\boldsymbol{F}}_s\hat{\boldsymbol{\Sigma}}\boldsymbol{n}_s = \mathbf{0}$ *on* $\partial\widehat{\Omega}_s\backslash\widehat{\Gamma}_i$ *hold. First, we get:*

$$\begin{aligned}\frac{d}{dt}\left[\frac{\rho_f}{2}||\boldsymbol{v}_f||^2_{\Omega_f(t)} + \frac{\hat{\rho}_s}{2}||\hat{\boldsymbol{v}}_s||^2_{\widehat{\Omega}_s} + \int_{\widehat{\Omega}_s} W(\hat{\boldsymbol{E}})\,d\hat{\boldsymbol{x}}\right]\\ + \gamma_w||\hat{\boldsymbol{v}}_s||^2_{\widehat{\Omega}_s} - \gamma_s(\partial_t\widehat{\boldsymbol{div}}(\hat{\boldsymbol{F}}_s\hat{\boldsymbol{\Sigma}}), \partial_t\hat{\boldsymbol{u}}_s)_{\widehat{\Omega}_s}\\ + 2\nu_f||\boldsymbol{D}(\boldsymbol{v_f})||^2_{\Omega_f(t)}\\ = 0.\end{aligned}$$

Second, the following energy decay property holds:

$$\begin{aligned}E(t) = E(0) - \int_0^t 2\nu_f||\boldsymbol{D}(\boldsymbol{v_f})||^2_{\Omega_f(t)}\,d\tau\\ - \int_0^t\left[\gamma_w||\hat{\boldsymbol{v}}_s||^2_{\widehat{\Omega}_s}\,d\tau - \gamma_s(\partial_\tau\widehat{\boldsymbol{div}}(\hat{\boldsymbol{F}}_s\hat{\boldsymbol{\Sigma}}), \partial_\tau\hat{\boldsymbol{u}}_s)_{\widehat{\Omega}_s}\,d\tau\right].\end{aligned}$$

The density of elastic energy W *is defined in [13]. From this relation, the constitutive stress tensor for the STVK material can be derived easily. The total energy of the coupled system at time step* t *is denoted by* $E(t)$.

2.6. Monolithic formulation of the coupled problem

The monolithic setting of the coupled equations of Problem 1 with 4 via the conditions in Eqn (3) is derived in the same manner as [27]. In particular, all equations are defined (and solved) in the reference configuration $\widehat{\Omega} = \widehat{\Omega}_f \cup \widehat{\Omega}_s$. To solve the non-linear problem, we introduce a semi-linear form and write in compact notation: Find $\hat{\boldsymbol{U}} = \{\hat{\boldsymbol{v}}, \hat{\boldsymbol{u}}, \hat{p}\} \in \hat{\boldsymbol{X}}$, where $\hat{\boldsymbol{X}}^0 := \{\hat{\boldsymbol{v}}^D + \hat{\boldsymbol{\mathcal{V}}}^0\} \times \{\hat{\boldsymbol{u}}^D + \hat{\boldsymbol{\mathcal{V}}}^0\} \times \hat{\mathcal{L}}$, such that

$$\int_0^T \hat{A}(\hat{\boldsymbol{U}})(\hat{\boldsymbol{\Psi}})\,dt = \int_0^T \hat{F}(\hat{\boldsymbol{\Psi}})\,dt \quad \forall\hat{\boldsymbol{\Psi}} \in \hat{\boldsymbol{X}}^0. \tag{5}$$

The linear form is given by $\hat{F}(\hat{\Psi}) \equiv 0$ because we neglect volume forces. The semi-linear form $\hat{A}(\hat{\boldsymbol{U}})(\hat{\boldsymbol{\Psi}})$ is defined by

$$\begin{aligned}\hat{A}(\hat{U})(\hat{\Psi}) = (\hat{J}\hat{\rho}_f\partial_t\hat{\boldsymbol{v}}, \hat{\boldsymbol{\psi}}^v)_{\widehat{\Omega}_f}\\ + (\hat{\rho}_f\hat{J}(\hat{\boldsymbol{F}}^{-1}(\hat{\boldsymbol{v}} - \hat{\boldsymbol{w}})\cdot\widehat{\boldsymbol{\nabla}})\hat{\boldsymbol{v}}), \hat{\boldsymbol{\psi}}^v)_{\widehat{\Omega}_f}\\ + (\hat{J}\hat{\boldsymbol{\sigma}}_f\widehat{\boldsymbol{F}}^{-T}, \widehat{\boldsymbol{\nabla}}\hat{\boldsymbol{\psi}}^v)_{\widehat{\Omega}_f} + (\hat{\rho}_s\partial_t\hat{\boldsymbol{v}}, \hat{\boldsymbol{\psi}}^v)_{\widehat{\Omega}_s}\\ + \gamma_w(\hat{\boldsymbol{v}}, \hat{\boldsymbol{\psi}}^v)_{\widehat{\Omega}_s} + \gamma_s(\partial_t\widehat{\mathbf{div}}(\hat{\boldsymbol{F}}_s\hat{\boldsymbol{\Sigma}}), \hat{\boldsymbol{\psi}}^v)_{\widehat{\Omega}_s}\\ + (\hat{J}\hat{\boldsymbol{\sigma}}_s\widehat{\boldsymbol{F}}^{-T}, \widehat{\boldsymbol{\nabla}}\hat{\boldsymbol{\psi}}^v)_{\widehat{\Omega}_s} + (\partial_t\hat{\boldsymbol{u}}, \hat{\boldsymbol{\psi}}^u)_{\widehat{\Omega}_s} - (\hat{\boldsymbol{v}}, \hat{\boldsymbol{\psi}}^u)_{\widehat{\Omega}_s}\\ + (\hat{\boldsymbol{\sigma}}_{\text{mesh}}, \widehat{\boldsymbol{\nabla}}\hat{\boldsymbol{\psi}}^u)_{\widehat{\Omega}_f} - \langle\hat{\boldsymbol{\sigma}}_{\text{mesh}}\hat{\boldsymbol{n}}_f, \hat{\boldsymbol{\psi}}^u\rangle_{\widehat{\Gamma}_i}\\ + (\widehat{\text{div}}\,(\hat{J}\widehat{\boldsymbol{F}}^{-1}\hat{\boldsymbol{v}}), \hat{\boldsymbol{\psi}}^p)_{\widehat{\Omega}_f} + (\hat{p}, \hat{\boldsymbol{\psi}}^p)_{\widehat{\Omega}_s}.\end{aligned} \tag{6}$$

3. Discretization

For temporal integration of Problem 5, we use the shifted Crank-Nicolson scheme based on finite differences that was developed for our ALE scheme in [26]. Spatial discretization in the reference configuration $\widehat{\Omega}$ is treated by a conforming Galerkin finite element scheme, leading to a finite dimensional subspace $\hat{\boldsymbol{X}}_h \subset \hat{\boldsymbol{X}}$. The discrete spaces are based on the Q_2^c/P_1^{dc} element for the fluid problem. The structure problem is discretized by the Q_2^c element. The non-linear problem is solved by the Newton method where the Jacobian is derived by exact linearization of the directional derivatives [26].

3.1. Residual based stabilization

Modeling blood flow at the exit of the aortic valve leads to a convection dominated problem with a Reynolds number ~ 4500 [15]. For this reason, we need to stabilize our formulation. The first ideas goes back to [6]. Our method of choice is a streamline upwind Petrov-Galerkin (SUPG) method. In the case of pure fluid problems it is a well-known drawback that additional boundary layers appear in the pressure approximation. This leads to a decrease in accuracy near the boundary. From computational point of view, the second disadvantage comes from the necessity to compute second derivatives because we are dealing with the strong formulation. Especially, in case of fluid-structure interaction problems this is a serious drawback. In our computations, we only used a simplified version because that worked fine in our numerical tests. The definition in $\Omega_f(t)$ reads:

$$\begin{aligned}&s_{\text{SUPG}}(\boldsymbol{U}_{kh})(\boldsymbol{\Psi})\\ &:= \sum_{m=1}^{M}\left\{\int_{I_m}\sum_{K\in\mathcal{T}_h^m}(\rho_f\boldsymbol{v}_f\cdot\boldsymbol{\nabla}\boldsymbol{v}_f, \delta_{K,m}(\boldsymbol{v}_{kh}\cdot\boldsymbol{\nabla})\boldsymbol{\psi}^v)_K\right\}\end{aligned}$$

with

$$\delta_{K,m} = \delta_0\frac{h_K^2}{6\nu_f + h_K||\boldsymbol{v}_{kh}||_K}, \quad \delta_0 = 0.1.$$

For more details on the choice of these parameters, we refer to [5].

4. Adaptive Mesh Refinement for Stationary Problems

To overcome the computational cost to solve our problem, especially due to the artificial layer, we discuss three different mesh refinement procedures to our problem. Because of the complexity of the overall problem, we study the quantitative aspects of mesh refinement only for stationary test cases. First results (to different steady-state configurations) from other authors are already known [8, 29, 22].

However, the first two refinement procedures (global and smoothness-based) have been used also for the non-stationary numerical examples. We use:

- Global mesh refinement;
- Smoothness-based mesh refinement;
- Goal-oriented mesh refinement with the dual weighted residual (DWR) method.

The first procedure is self-explaining. For the second type, we measure the jumps of the first derivatives over edges, which corresponds to a measure of the smoothness of the discrete solution. The third type will be subject of the discussion in the following. For coupled problems this formulation is still under investigation and becomes costly for space-time dependent problems. For this reason, we test our configuration in a stationary setting, where we only scale the inflow velocity such that a steady state solution is obtained.

4.1. Goal oriented mesh adaption with the DWR method

The Galerkin approximation to Problem 5 (neglecting the time derivatives and stabilization terms), reads: Find $\hat{\boldsymbol{U}}_h = \{\hat{\boldsymbol{v}}_h, \hat{\boldsymbol{u}}_h, \hat{p}_h\} \in \hat{\boldsymbol{X}}_h$, where $\hat{\boldsymbol{X}}^0 := \{\hat{\boldsymbol{v}}^D + \hat{\boldsymbol{\mathcal{V}}}^0\} \times \{\hat{\boldsymbol{u}}^D + \hat{\boldsymbol{\mathcal{V}}}^0\} \times \hat{\mathcal{L}}$, such that

$$\hat{A}(\hat{\boldsymbol{U}}_h)(\hat{\boldsymbol{\Psi}}_h) = \hat{F}(\hat{\boldsymbol{\Psi}}_h) \quad \forall \hat{\boldsymbol{\Psi}}_h \in \hat{\boldsymbol{X}}_h^0. \tag{7}$$

The solution $\hat{\boldsymbol{U}}_h$ is used to calculate an approximation $J(\hat{\boldsymbol{U}}_h)$ of the goal-functional $J(\hat{\boldsymbol{U}})$. This functional can be evaluation of point values (deflection of the valve), line integrals (computation of stresses), or domain integrals. To derive an computable representation of the approximation error $J(\hat{\boldsymbol{U}}) - J(\hat{\boldsymbol{U}}_h)$, we introduce a dual variable $\hat{\boldsymbol{Z}}$, and obtain [4]:

Lemma 4.1. *For any solution of Eqn* (5) *and 7, we have the error representation*

$$\begin{aligned} &J(\hat{\boldsymbol{U}}) - J(\hat{\boldsymbol{U}}_h) \\ =&\frac{1}{2}\rho(\hat{\boldsymbol{U}}_h)(\hat{\boldsymbol{Z}} - \hat{\boldsymbol{\Psi}}_h) + \frac{1}{2}\rho^*(\hat{\boldsymbol{U}}_h, \hat{\boldsymbol{Z}}_h)(\hat{\boldsymbol{U}} - \hat{\boldsymbol{\Phi}}_h) + \mathcal{R}_h^{(3)} \end{aligned}$$

for all $\{\hat{\boldsymbol{\Phi}}_h, \hat{\boldsymbol{\Psi}}_h\} \in \hat{\boldsymbol{X}}_h \times \hat{\boldsymbol{X}}_h$ *and with the primal and dual residuals:*

$$\begin{aligned} \rho(\hat{\boldsymbol{U}}_h)(\hat{\boldsymbol{Z}} - \hat{\boldsymbol{\Psi}}_h) &:= -A(\hat{\boldsymbol{U}}_h)(\cdot), \\ \rho^*(\hat{\boldsymbol{U}}_h, \hat{\boldsymbol{Z}}_h)(\hat{\boldsymbol{U}} - \hat{\boldsymbol{\Phi}}_h) &:= J'(\hat{\boldsymbol{U}}_h)(\cdot) - A(\hat{\boldsymbol{U}}_h)(\cdot, \hat{\boldsymbol{Z}}_h) \end{aligned}$$

The remainder term is $\mathcal{R}_h^{(3)}$ *is cubic in the primal and dual errors. This error identity can be used to drive an automatic mesh refinement process and/or can be adopted to estimate the error.*

The dual variable $\hat{\boldsymbol{Z}}$ is computed by the corresponding (linearized) dual problem

$$A(\hat{\boldsymbol{\Psi}}_h, \hat{\boldsymbol{Z}}_h) = J(\hat{\boldsymbol{\Psi}}_h), \quad \forall \hat{\boldsymbol{\Psi}}_h \in \hat{\boldsymbol{X}}_h. \tag{8}$$

The dual Problem 8 can be solved by global higher approximation or local higher interpolation. To obtain a 'computable' version of the error identity, we set up some assumptions. First, we neglect the remainder term $\mathcal{R}_h^{(3)}$. Second, we are only interested in automatic mesh refinement and we use only the primal residual to estimate the error. Moreover, we neglect the structure damping terms because their influence in stationary setting is sufficient small. Fourth, we transform (as originally suggested) the error identity by cell-wise partial integration into the strong form, leading to challenging structure of the Laplacian term of the fluid equations. Because, we are only dealing with moderate deformations, we assume (while computing the error) that $\widehat{\boldsymbol{F}} = \boldsymbol{I}$ and $J = 1$, and a symmetric stress tensor:

$$(\hat{J}\hat{\boldsymbol{\sigma}}_{lap}\widehat{\boldsymbol{F}}^{-T}, \widehat{\boldsymbol{\nabla}}\hat{\boldsymbol{\psi}}^v)_{\widehat{\Omega}_f},\ \hat{\boldsymbol{\sigma}}_{lap} := \hat{\rho}_f\nu_f(\widehat{\boldsymbol{\nabla}}\hat{\boldsymbol{v}}_f\widehat{\boldsymbol{F}}^{-1} + \widehat{\boldsymbol{F}}^{-T}\widehat{\boldsymbol{\nabla}}\hat{\boldsymbol{v}}_f^T),$$

leading to

$$(\hat{\boldsymbol{\sigma}}_{lap}, \widehat{\boldsymbol{\nabla}}\hat{\boldsymbol{\psi}}^v)_{\widehat{\Omega}_f},\ \hat{\boldsymbol{\sigma}}_{lap} := \hat{\rho}_f\nu_f(\widehat{\boldsymbol{\nabla}}\hat{\boldsymbol{v}}_f).$$

This can be transformed easily into the strong formulation. Basically, the same idea is used for the constitutive tensor of the structure:

$$(\widehat{\boldsymbol{F}}\widehat{\boldsymbol{\Sigma}}_s, \widehat{\boldsymbol{\nabla}}\hat{\boldsymbol{\psi}}^v)_{\widehat{\Omega}_s},\ \widehat{\boldsymbol{\Sigma}}_s := (\lambda_s(\mathrm{tr}\widehat{\boldsymbol{E}})\boldsymbol{I} + 2\mu_s\widehat{\boldsymbol{E}}).$$

The structure tensor is approximated by

$$\begin{aligned} \widehat{\boldsymbol{\Sigma}}_s &:= (\lambda_s(\mathrm{tr}\widehat{\boldsymbol{E}})\boldsymbol{I} + 2\mu_s\widehat{\boldsymbol{E}}) \approx 2\mu_s\widehat{\boldsymbol{E}} \\ &\approx 2\mu_s\frac{1}{2}(\widehat{\boldsymbol{\nabla}}\hat{\boldsymbol{u}} + \widehat{\boldsymbol{\nabla}}\hat{\boldsymbol{u}}^T) \approx (\mu_s\widehat{\boldsymbol{\nabla}}\hat{\boldsymbol{u}}). \end{aligned}$$

From this, we obtain the following (simplified) error representation:

$$\begin{aligned} &J(\hat{\boldsymbol{U}}) - J(\hat{\boldsymbol{U}}_h) \approx \rho(\hat{\boldsymbol{U}}_h)(\hat{\boldsymbol{Z}} - \hat{\boldsymbol{\Psi}}_h) \\ :=& \sum_{\widehat{K}\in\mathcal{T}_h} \{(-\hat{\rho}_f\hat{J}(\widehat{\boldsymbol{F}}^{-1}(\hat{\boldsymbol{v}} - \hat{\boldsymbol{w}})\cdot\widehat{\boldsymbol{\nabla}})\hat{\boldsymbol{v}} + \rho_f\nu_f\Delta\boldsymbol{v}_h, \hat{\boldsymbol{z}}^v - \hat{\boldsymbol{\psi}}_h^v)_{\widehat{K}_f} \\ &+ \frac{1}{2}([\hat{J}\hat{\boldsymbol{\sigma}}_f\widehat{\boldsymbol{F}}^{-T}\hat{\boldsymbol{n}}_f], \hat{\boldsymbol{z}}^v - \hat{\boldsymbol{\psi}}_h^v)_{\partial\widehat{K}_f\setminus\partial\widehat{\Omega}} \\ &+ (\widehat{\mathrm{div}}\,(\hat{J}\widehat{\boldsymbol{F}}^{-1}\hat{\boldsymbol{v}}), \hat{\boldsymbol{z}}^p - \hat{\boldsymbol{\psi}}_h^p)_{\widehat{K}_f} \\ &+ (\widehat{\boldsymbol{\sigma}}_{\mathrm{mesh}}, \hat{\boldsymbol{z}}^u - \hat{\boldsymbol{\psi}}_h^u)_{\widehat{K}_f} \\ &+ \frac{1}{2}([\widehat{\boldsymbol{\sigma}}_{\mathrm{mesh}}\hat{\boldsymbol{n}}_f], \hat{\boldsymbol{z}}^u - \hat{\boldsymbol{\psi}}_h^u)_{\partial\widehat{K}_f\setminus\partial\widehat{\Omega}} \\ &+ (\mu_s\Delta\hat{\boldsymbol{u}}_h, \hat{\boldsymbol{z}}^v - \hat{\boldsymbol{\psi}}_h^v)_{\widehat{K}_s} \\ &+ \frac{1}{2}([\widehat{\boldsymbol{\sigma}}_s\hat{\boldsymbol{n}}_s], \hat{\boldsymbol{z}}^v - \hat{\boldsymbol{\psi}}_h^v)_{\partial\widehat{K}_s\setminus\partial\widehat{\Omega}} \\ &- (\hat{\rho}_s\hat{\boldsymbol{v}}_h, \hat{\boldsymbol{z}}^u - \hat{\boldsymbol{\psi}}_h^u)_{\widehat{K}_s} - (\hat{p}, \hat{\boldsymbol{z}}^p - \hat{\boldsymbol{\psi}}_h^p)_{\widehat{K}_s}. \end{aligned}$$

Remark 4.1. Using the strong formulation for the error computation might be costly for the DWR method in space and time. Especially, one should not neglect the transformation around the Laplacian. How this can be achieved in an efficient way, is still an open question for fluid-structure interaction problems.

5. Numerical Tests

We discuss two numerical examples that are based on the same configuration and parameters. We start by presenting a prototypical unsteady heart valve simulation. Our aim is to verify the proposed structure outflow conditions. To this end, the valves have sufficient distance to avoid touching and resulting difficulties.

Because we extend the channel to compute the damped wave equation that can absorb out-coming waves, one major disadvantage is the computational cost. This can be overcome with (at least) two different solutions. First, we use a (hand-made) coarser mesh in the artificial domain. Second, which brings us to the numerical Example 2, we use automatic adaptive mesh refinement with the DWR method.

The (reference) configuration $\widehat{\Omega}$ of the test case is illustrated in Fig. 1.

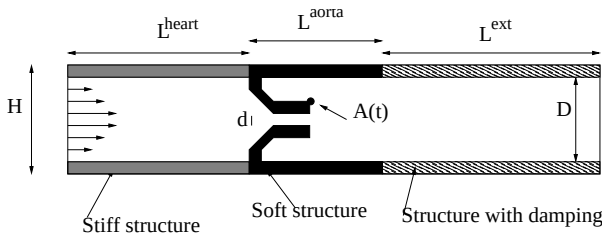

Figure 1: Configuration (in cm): $L^{heart} + L^{aorta} = 6.0, L^{ext} = 12, H = 2.9, D = 2.5, d = 0.1$.

Inflow and boundary conditions

A time dependent parabolic velocity inflow profile is prescribed on $\hat{\Gamma}_{in}$ (left boundary H), sketched in Fig. 2, for the first test case. This inflow profile is scaled by a constant factor 0.1. For the second test, we choose a constant inflow velocity $\hat{\boldsymbol{v}}^D = 10cm/s$ leading to a steady-state solution.

The 'do-nothing' condition is used on $\hat{\Gamma}_{out}$ (right boundary D in Fig. 1).

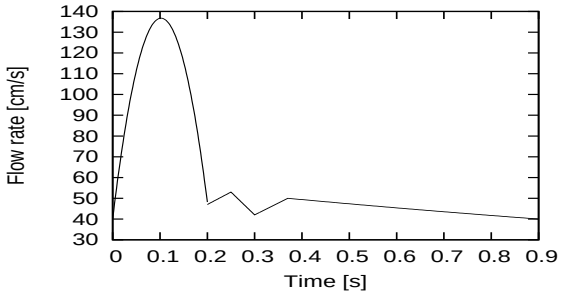

Figure 2: Interpolated flow rate profile for one cardiac cycle.

The structure is fixed at $\hat{\Gamma}_{in}$ and $\hat{\Gamma}_{out}$ and it is left free at the outer elastic walls, to allow them to move.

Quantities of comparison and their evaluation

We evaluate the deflections in both x- and y-direction at the tails of one heart valve at the point $A(0) = (3.64, 0.35)$, and the wall stresses at the upper wall between fluid and structure in the aorta (over the length L^{aorta}).

Parameters

For the fluid, we use density $\rho_f = 1gcm^{-3}$, and the viscosity $\nu_f = 0.03cm^2s^{-1}$. The elastic structure is characterized by the density $\rho_s = 1gcm^{-3}$, the Poisson ratio $\nu_s = 0.3$, and the Lamé coefficients $\mu_{heart} = 10^8gcm^{-1}s^{-2}$, $\mu_{valve} = 5.0 * 10^5gcm^{-1}s^{-2}$, $\mu_{aorta} = 10^6gcm^{-1}s^{-2}$. The (weak) damping parameter is given by $\gamma_w = 10^4$, the other one $\gamma_s = 0$.

Results of Test 1

One cardiac cycle has time length $T = [0s, 0.9s]$. Four time cycles are used to run the computation. The time step sizes are chosen in a range of $t = 0.02s - 0.002s$ to detect convergence with respect to time. We solve the problem on three different mesh levels to observe space convergence. The results are illustrated in Table 1.

The qualitative behavior of the solution can be studied in Fig. 3. The qualitative behavior for other damping parameters γ_w are discussed in [27].

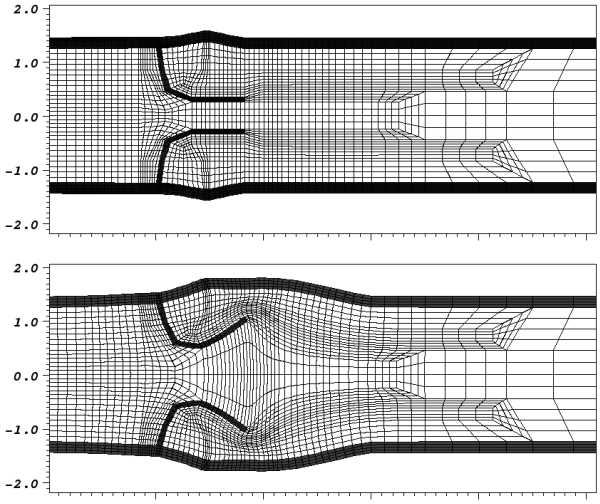

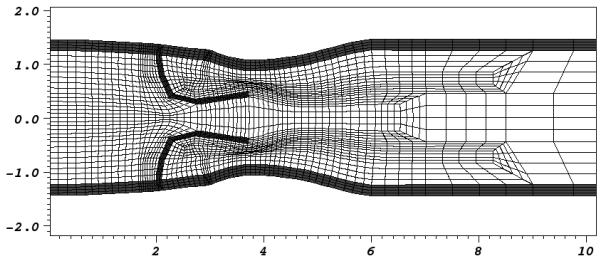

Figure 3: Grids of the long axis of the aortic heart valve at three different time steps $t_1 = 0s$, $t_2 = 0.130s$, and $t_3 = 0.350s$.

In Fig. 4, we observe the same qualitative behavior of the physical quantities for the last three cardiac cycles.

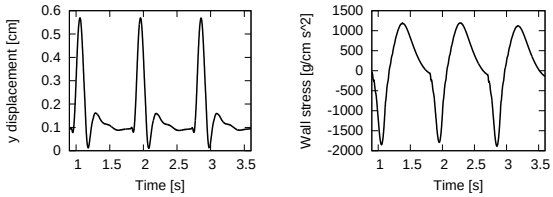

Figure 4: Evaluation of y-displacement at $A(t)$ and wall stress in y-direction along the upper wall of L^{aorta}.

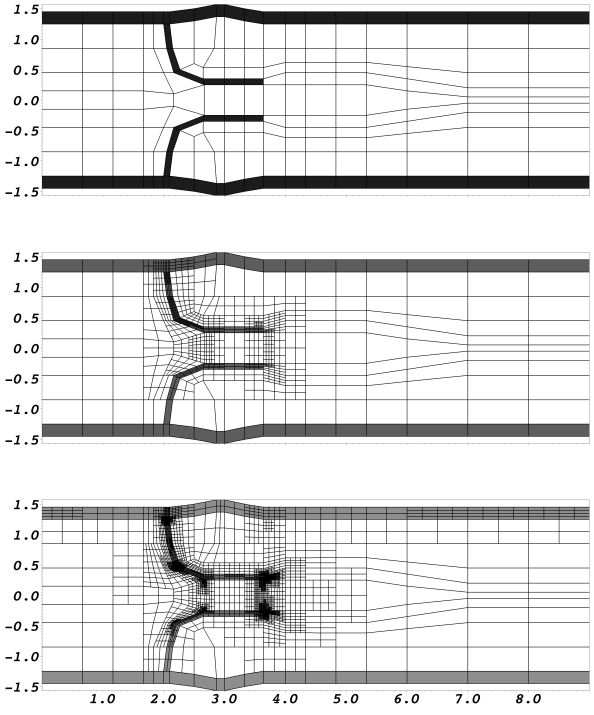

Figure 5: Meshes with 188, 926, and 4685 cells obtained by the Dual Weighted Residual estimator.

Table 1: Results for the first numerical test. Left: y displacement of point $A(t)$, measured in $[cm]$. Right: results for the measurement of the wall stresses in y direction, measured in $[gcm^{-1}s^{-2}]$

		Deflections in y direction		Wall stresses in y direction	
DoF	$k[s]$	max	min	max	min
5553	0.02	0.4745	0.03222	1075.85	−1763.74
5553	0.002	0.2225	0.01244	979.261	−1644.37
5553	0.001	0.1467	0.00372	865.705	−1423.05
21522	0.02	0.5395	0.00200	1060.42	−1783.44
21522	0.002	0.5676	0.01102	1116.00	−1884.87
21522	0.001	0.5651	0.01068	1116.59	−1887.65
84726	0.002	0.5501	−0.0454	1106.27	−1867.74
84726	0.001	0.5477	−0.0440	1109.84	−1869.06

Table 2: Numerical Test 2: Displacements of the control point A for a sequence of mesh levels of locally refined meshes with the DWR method

Cells	DoF	$A(x)[10^{-4}cm]$	$A(y)[10^{-4}cm]$
188	3996	2.6153	8.7667
233	5136	2.6921	9.1156
479	10556	2.7576	9.1793
926	20232	2.7674	9.1706
1721	37484	2.7700	9.1636
2882	62912	2.7742	9.1629
4685	101804	2.7763	9.1621

Results of Test 2

In this test case, we consider a steady-state solution to our problem by scaling the inflow profile. In Table 2 the deflections in both principal directions are displayed for a sequence of locally refined meshes with the DWR method.

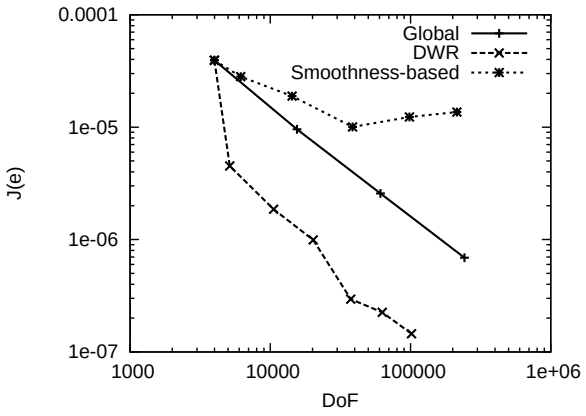

Figure 6: Error of the point y-evaluation at the tail $A(t)$ of the upper valve versus number of degrees of freedom, for uniform refinement, the weighted indicator obtained by the Dual Weighted Residual method, and smoothness-based indicators.

A comparison between the three proposed refinement types is made in Fig. 6. The reference value for the error determination is computed on a very fine mesh obtained by global refinement and extrapolation of the solution. We monitor the same convergence rate for both global refinement and mesh adaption with the DWR method. However, we detect a better constant when using the DWR method. The corresponding meshes are displayed in Fig. 5 for three exemplary solutions. The (heuristic) indicator performs worse than the other two procedures and is no option for this numerical test case.

6. Conclusions

In this work, we proposed a monolithic fluid-structure framework to simulate a two-dimensional long axis heart valve. The computational domain was prolongated by an artificial layer to prevent backflow of structure waves. To reduce computational cost, we developed a simplified DWR estimator for mesh adaption. We plan to extend this concept to time dependent cases. In further studies, we will investigate the influence of the damping parameters. Moreover, we plan to couple the model with absorbing boundary conditions for the fluid part.

References

[1] Bangerth, W., Hartmann, R., Kanschat, G., Differential Equations Analysis Library, *Technical Reference*, 2010. `http://www.dealii.org`

[2] Bangerth, W., Grothe, M., Hohenegger, Ch., Finite element method for time dependent scattering: nonreflecting boundary conditionm, adaptivity, and energy decay, *Comp. Meth. Appl. Mech. Engng.*, 193, pp. 2453–2482, 2004.

[3] Berenger, J.-P., A perfectly matched layer for the absorption of electromagnetic waves, *J. Comput. Phys.*, 114, No. 185, 1994.

[4] Becker, R. and Rannacher, R., An optimal control approach to error control and mesh adaptation in finite element methods, *Acta Numerica 2001*, (A. Iserles, ed.), Cambridge University Press, 2001.

[5] Braack, M., Burman, E., John, V., Lube, G., Stabilized finite element methods for the generalized Oseen equations, *Comput. Methods Appl. Mech. Engrg.*, 196(4–6), pp. 853–866, 2007.

[6] Brooks, A. N., Hughes, T. J. R., Streamline upwind/Petrov-Galerkin formulations for convection dominated flows with particular emphasis on the incompressible Navier-Stokes equations, *Comput. Methods Appl. Mech. Engrg.*, 32(1–3), pp. 199–259, 1982.

[7] Causin, P., Gerbeau, J.-F., Nobile, F., Added-mass effect in the design of partitioned algorithms for fluid-structure problems, *Comput. Methods Appl. Mech. Engrg.*, 194, pp. 4506–4527, 2005.

[8] Dunne, T., Rannacher, R., Richter, T., Numerical Simulation of Fluid-Structure Interaction Based on Monolithic Variational Formulations, *Numerical Fluid Structure Interaction*, G.P. Galdi, R. Rannacher et. al, Springer, 2010.

[9] Engquist, B., Majda, A., Absorbing boundary conditions for the numerical simulation of waves, *Math. Comp.*, 31, No. 139, pp. 629–651, 1977.

[10] Figueroa, C.A., Vignon-Clementel, I.E., Jansen, K.E., Hughes, T.J.R., Taylor, C.A., A coupled momentum method for modeling blood ïňĆow in three-dimensional deformable arteries, *Comput. Methods Appl. Mech. Engrg.*, 195, pp. 5685–5706, 2006.

[11] Formaggia, L., Moura, A., Nobile, F., On the stability of the coupling of 3D and 1D fluid-structure interaction models for blood flow simulations, *Technical Report at MOX*, 94, 2006.

[12] Formaggia, L., Gerbeau, J.-F., Nobile, F., Quarteroni, A., On the Coupling of 3D and 1D Navier-Stokes equations for Flow Problems in Compliant Vessels, *Comp. Meth. Appl. Mech. Engng.*, 191, pp. 561–582, 2001.

[13] Formaggia, L., Quarteroni, A., Veneziani, A., *Cardiovascular Mathematics: Modeling and simulation of the circulatory system*, Springer-Verlag, Italia, Milano, 2009.

[14] Formaggia, L., Veneziani, A., Vergara, Ch., Flow rate boundary problems for an incompressible fluid in deformable domains: formulations and solution methods, *Comput. Meth. Appl. Mech. Engrg.*, 199, pp. 677–688 (2010).

[15] Fung, Y.C., *Biodynamics: Circulation*, first ed., Springer-Verlag, 1984.

[16] Janela, J., Moura, A., Sequeira, A., Absorbing boundary conditions for a 3D non-Newtonian fluid-structure interaction model for blood flow in arteries, *Int. J. Engrg. Sci.*, 2010.

[17] Jianhai, Z., Dapeng, C., Shengquan, Z., ALE finite element analysis of the opening and closing process of the artificial mechanical valve, *Applied Math. Mech.*, 17(5), pp. 403–412, 2006.

[18] Mizerski, J., Discussions on Heart Valve Modeling, *Personal correspondance to the author*, 2010.

[19] Nobile, F., Vergara, C., An Effective Fluid-Structure Interaction Formulation for Vascular Dynamics by Generalized Robin Conditions, *SIAM J. Sci. Comput.*, v.30 n.2, pp. 731–763, 2008.

[20] Peskin, C., The immersed boundary method, *Acta Numerica*, Cambridge University Press, pp. 1–39, 2002.

[21] Quarteroni, A., What mathematics can do for the simulation of blood circulation, *MOX Report*, 2006.

[22] Richter, T., Adaptive Finite Elements for 3D Fluid-Structure Interaction Problems, *submitted*, 2011.

[23] Diniz Dos Santos, N., Gerbeau, J.-F., Bourgat, J.F., A partitioned fluid-structure algorithm for elastic thin valves with contact, *Comp. Meth. Appl. Mech. Engng.*, Vol. 197, Num. 19-20, pp. 1750–1761, 2008.

[24] Le Tallec, P., Mouro, J., Fluid structure interaction with large structural displacements, *Comput. Meth. Appl. Mech. Engrg.*, 190, pp. 3039–3067, 2001.

[25] Vierendeels, J., Dumont, K., Verdonck, P.R., A partitioned strongly coupled fluid-structure interaction method to model heart valve dynamics, *J. Comp. Appl. Math.*, 2008.

[26] Wick, T., Fluid-Structure Interactions using Different Mesh Motion Techniques, *Computers and Structures*, in press, 2011.

[27] Wick, T., Energy absorbing layer for the structure outflow boundary in Fluid-structure interaction for heart valve dynamics, *submitted*, 2011.

[28] Wloka., J., *Partielle Differentialgleichungen*, B.G. Teubner, Stuttgart, 1987.

[29] van der Zee, K. G., van Brummelen E. H., de Borst, R., Goal-oriented error estimation for Stokes flow interacting with a flexible channel, *Int. J. Numer. Meth. Fluids*, 56, pp. 1551–1557, 2008.